Earth and Planetary Science Letters 290 (2010) 224–232

Contents lists available at ScienceDirect

Earth and Planetary Science Letters

journal homepage: www.elsevier.com/locate/epsl

Small-scale sublithospheric convection reconciles geochemistry and geochronology of 'Superplume' volcanism in the western and south Pacific

Maxim D. Ballmer [a,*], Garrett Ito [b], Jeroen van Hunen [c], Paul J. Tackley [a]

[a] Institute of Geophysics, ETH Zürich, Sonneggstrasse 5, 8092 Zürich, Switzerland
[b] School of Ocean and Earth Sciences and Technology, University of Hawaii, 1680 East-West Road, Honolulu, USA
[c] Department of Earth Sciences, Durham University, DH1 3LE, Durham, UK

ARTICLE INFO

Article history:
Received 9 June 2009
Received in revised form 7 December 2009
Accepted 9 December 2009
Available online 12 January 2010

Editor: Y. Ricard

Keywords:
small-scale convection
intraplate volcanism
mantle heterogeneity
South Pacific
Darwin Rise

ABSTRACT

Cretaceous volcanism in the West Pacific Seamount Province (WPSP), and Tertiary volcanism along the Cook-Australs in the South Pacific are associated with the same broad thermochemical anomaly in the asthenosphere perhaps related to the Pacific 'Superplume.' Abundant volcanism has usually been attributed to secondary plumelets rising from the roof of the Superplume. The Cook-Australs display distinct geochemical trends that appear to geographically project, backward in time, to corresponding trends in the WPSP. However, the implied close proximity of source regions (i.e., ~1000 km) with very different geochemical fingerprints and their longevity over geological time (>100 Myrs) appear to be at odds with the secondary plumelet hypothesis, a mechanism with a typical timescale of ~30 Myrs. Moreover, ages sampled along the individual volcano chains of the Cook-Australs, and of the WPSP violate the predictions of the plumelet hypothesis in terms of linear age–distance relationships.

Our numerical models indicate that small-scale sublithospheric convection (SSC) as likely triggered by the thermochemical anomaly of the 'Superplume' instead reconciles complex age–distance relationships, because related volcanism occurs above elongated melting anomalies parallel to plate motion ('hot lines'). Furthermore, SSC-melting of a mantle source that consists of pyroxenite veins and enriched peridotite blobs in a matrix of depleted peridotite creates systematic geochemical trends over seafloor age during volcanism. These trends arise from variations in the amount of pyroxenite-derived lavas relative to peridotite-derived lavas along a 'hot line,' therefore stretching between the geochemical end-members HIMU and EMI. These predicted trends are consistent with observed trends in radiogenic isotopic composition from the Wakes, Marshalls, Gilberts (i.e., the individual volcano groups of the WPSP) and the Cook-Australs. For increasing mantle temperatures, volcanism is further predicted to occur at greater seafloor ages and with a more EMI-like signature, a result that can explain many of the observed systematics. Thus, SSC explains many of the geochemical observations with long-term temporal variations in mantle temperature, instead of persistent intermediate-scale (~1000 km) compositional heterogeneity.

1. Introduction

The origin of oceanic intraplate volcanism is still debated today. While classical plume theory successfully explains many observations at some long-lived volcano chains with a linear age–distance relationship (Morgan, 1972), it does not give an explanation for the spectrum of observations at many short-lived volcano chains (e.g., Courtillot et al., 2003). While these discrepancies have urged some authors to abandon plume theory altogether (Anderson, 2000; Foulger, 2007), others invoke a variety of mechanisms to account for the spectrum of intraplate volcanism. Short-lived chains were attributed to secondary plumelets that detach from the top of a major diffuse upwelling (i.e., a Superplume) (Davaille, 1999), or to various non-hotspot mechanisms (King and Ritsema, 2000; Koppers et al., 2003; King, 2007; Clouard and Gerbault, 2008a; Ballmer et al., 2009). Illuminating the geodynamical mechanisms and the related processes of partial melting is essential in order to understand the observed geochemical characteristics of ocean island basalts (OIBs), and ultimately the composition of the mantle source.

The South Pacific (SP) is an unusual location, where multiple active parallel volcano chains with a short lifetime (~30 Myrs) are concentrated. Geochemical arguments (Staudigel et al., 1991), constraints from seismic tomography (e.g., Ritzwoller and Lavely, 1995), and most importantly, a broad topographic swell (McNutt and Fisher, 1987) suggest that the region is underlain by a thermochemical anomaly, possibly the expression of a giant diffuse mantle upwelling — the SP Superplume (Larson, 1991).

The West Pacific Seamount Province (WPSP) includes the Wakes, Marshalls and Gilberts and is located on the topographical swell of the

* Corresponding author. Tel.: +41 44 632 0244; fax: +41 44 633 1065.
E-mail address: ballmer@tomo.ig.erdw.ethz.ch (M.D. Ballmer).

0012-821X/$ – see front matter © 2009 Elsevier B.V. All rights reserved.
doi:10.1016/j.epsl.2009.12.025

Darwin Rise, a feature that has been interpreted as the Cretaceous analogue of the SP Superswell (McNutt and Fisher, 1987; Wolfe and McNutt, 1991; Ritzwoller and Lavely, 1995). In further support of this notion is the suggestion that volcanoes in the Cretaceous WPSP and the Tertiary Cook-Australs (a double chain located at the southern edge of the SP Superswell) share a common mantle source, both geographically (Larson, 1991; Konter et al., 2008) and geochemically (Davis et al., 1989; Staudigel et al., 1991; Janney and Castillo, 1999; Koppers et al., 2003). Thus, the WPSP and the Cook-Australs likely originated from similar geodynamic processes perhaps related to the Superplume.

The geochemical link between the WPSP and the Cook-Australs is an important clue to the originating processes. Geochemical compositions of Cook-Austral basalts project along distinct trends between the geochemical end-members EM1 and HIMU, as well as DMM and C/FOZO (Zindler and Hart, 1986; Staudigel et al., 1991; Hart et al., 1992; Hanan and Graham, 1996; Bonneville et al., 2006). Accordingly, these trends span almost the whole OIB array on an area that covers only ~0.14% of the Earth's surface. Distinct geochemical trends of the Cook-Australs appear to geographically project, backward in time, to corresponding trends in the WPSP (Konter et al., 2008). The implied spatial longevity of very distinct geochemical sources over geological time (>100 Myrs) has been ascribed to a strongly heterogeneous mantle domain within the Superplume, which rose from the lowermost mantle (e.g., subduction graveyard) (Konter et al., 2008). However, it appears to be unlikely that the close proximity (<1000 km) and the longevity (>100 Myrs) of the geochemical anomalies may be explained by a mechanism with a typical timescale of ~30 Myrs such as secondary plumelets.

Moreover, the predictions of the plumelet hypothesis appear to be very difficult to reconcile with volcano ages sampled. To explain all sample ages at the Cook-Australs, at least three (Bonneville et al., 2006) or likely even more plumelets (McNutt et al., 1997; Clouard and Bonneville, 2005; Clouard and Gerbault, 2008b) would have to be invoked. For each individual chain of the WPSP, recent $^{39}Ar/^{40}Ar$ dating reveals highly complex and irregular age–distance relationships (Koppers et al., 2003, 2007), while the plumelet hypothesis implies short but regular age progressions coinciding with plate motion.

Small-scale sublithospheric convection (SSC) is one, among several non-hotspot processes proposed to create intraplate oceanic volcanism (e.g., see discussion in Ballmer et al., 2009). SSC evolves from instabilities of the cold and dense thermal boundary layer at the bottom of the oceanic lithosphere. Once evolved, SSC tends to organize as 'Richter' rolls that align with plate motion (Richter and Parsons, 1975). SSC typically establishes itself beneath oceanic seafloor of age ~70 Myrs (Parsons and McKenzie, 1978; Fleitout and Yuen, 1984; Stein and Stein, 1992; Doin and Fleitout, 2000), but it may be triggered significantly earlier in the presence of unusually low ambient mantle viscosity or lateral density heterogeneity (Huang et al., 2003; Dumoulin et al., 2008). The SP Superplume provides both these triggers (Staudigel et al., 1991; Cadek and Fleitout, 2003) therefore potentially giving rise to SSC (Griffiths and Campbell, 1991; Keller and Tackley, 2009). Such a situation may spawn decompression melting within the upwelling limbs of SSC (Fig. 1) (Bonatti and Harrison, 1976; Buck and Parmentier, 1986; Ballmer et al., 2007, 2009). Ballmer et al. (2007, 2009) showed that SSC of a homogeneous peridotitic mantle can create volcanoes of heights comparable to those in the WPSP and Cook-Australs in regions with low asthenospheric viscosity. However, such a peridotitic source alone is unable to produce parental melts for ocean island basalts (Niu and O'Hara, 2003).

In order to further examine the SSC hypothesis for 'Superplume' volcanism, we build upon our prior work (Ballmer et al., 2007, 2009) by exploring melting of a lithologically heterogeneous (i.e., veined) mantle. We compare model predictions in terms of isotope compositions of magmas produced, and age–distance relationships of volcanism to observations from the Wakes, Marshalls, Gilberts, and Cook-Australs. Finally, we discuss the role of thermal and compositional heterogeneity in the mantle source.

2. Methods and model description

We perform 3D-thermochemical numerical experiments using an extended version of the finite element code CITCOM (Moresi and Gurnis, 1996; Zhong et al., 2000). We solve the equations of mass, momentum, and energy of an incompressible, infinite Prandtl-number fluid, and use the extended Boussinesq approximation in order to consider the effects of latent heat of melt (with the specific latent heat $L=560$ kJ/kg), adiabatic heating (with the adiabatic gradient $\gamma=0.38882$ K/km), and viscous dissipation (Christensen and Yuen, 1985). Details of the numerical method used, and any unreported parameters are equivalent to those in Ballmer et al. (2009).

Calculations are performed in a Cartesian box cooled from above and heated from below. We impose a velocity boundary condition of +65 km/Myr at the top side in order to simulate Pacific plate motion. To accommodate the resulting flow, we allow inflow at the front side, which is parallel to, but 1170–2080 km away from the mid-ocean ridge (MOR), and outflow at the back side. The box is 3400 km long, 400 km deep, and 520 km wide using 448x56x64 elements. We impose +10 km/Myr at the bottom boundary to simulate a small amount of motion relative to the lower mantle (which is conceptually at 660, and not at 400 km depth). We close the bottom to prevent artificially large vigor, and long wavelength SSC. The plate motion parallel sides are free-slip boundaries.

Following the mantle marble-cake hypothesis, we model melting of a veined mantle source consisting of multiple lithologies (Allègre et al., 1984; Phipps Morgan, 2001; Ito and Mahoney, 2005a,b; Sobolev et al., 2007). We consider a lithological assemblage that consists of veins of pyroxenite (PX) and blobs of geochemically enriched peridotite with high volatile content ('enriched component,' EC)

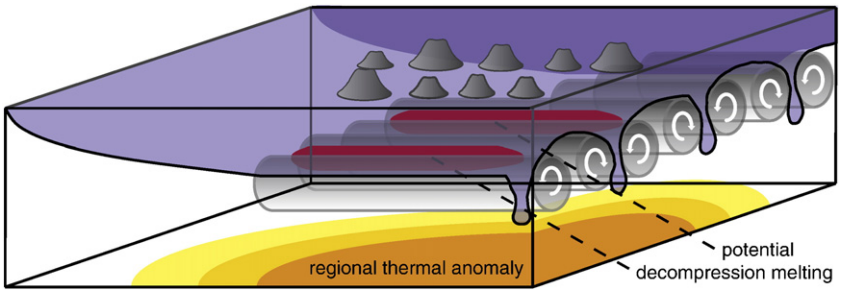

Fig. 1. Small-scale sublithospheric convection (SSC) spontaneously evolves at the bottom of mature oceanic lithosphere with a preferred geometry of rolls parallel to plate motion. SSC may be triggered earlier than elsewhere by influence of a regional thermal anomaly. Such a situation potentially yields decompression melting along the upwelling limbs of SSC, something that spawns 'hot line' volcanism.

both residing in a matrix of peridotite with low volatile content ('depleted component,' DC). For this assemblage, we assume thermal equilibrium and chemical disequilibrium during melting (cf. Ito and Mahoney, 2005a). To establish a reference case, we assume arbitrarily that the assemblage is divided into initial volume percentages of PX, EC, and DC of $\Phi_{PX,i}=4\%$, $\Phi_{EC}=16\%$, and $\Phi_{DC}=80\%$, respectively. Such a fertile bulk composition is chosen to simulate an upper mantle that is influenced by a Superplume (Staudigel et al., 1991).

For calculating peridotite melting temperatures, we use a version of the hydrous melting law from Katz et al. (2003) as modified in Ballmer et al. (2009). Water contents of the components prior to melting of $c_{O,DC}=0.0075$ wt.% for DC and $c_{O,EC}=0.04$ wt.% for EC yield a bulk water content that is comparable to estimates of the mantle beneath most mid-ocean ridges (Hirth and Kohlstedt, 1996). The difference in water concentrations causes a significant solidus reduction (of 87 °C) for EC relative to DC. The melting law applied for PX is taken from Pertermann and Hirschmann (2003).

We adopt the dynamic melting approximation (McKenzie, 1985), in which melt is retained in the solid matrix without migrating until the fraction of melt from each lithology reaches a critical porosity φ_C. Any exceeding melts from that lithology are instantaneously extracted to the surface, a model that neglects reaction between melt and solid during melt migration (in accord with U-series constraints (Stracke et al., 2006)). We take $\varphi_C=0.5\%$ in this reference model, a compromise between geochemical models (Stracke et al., 2006), and seismological observations (e.g., Toomey et al., 2002).

In our thermochemical models, density is a function of temperature and composition:

$$\rho-\rho_m = \alpha\rho_m(T-T_m) + \Phi_{EC}(\varphi_{EC}\Delta\rho_\varphi + F_{EC}\Delta\rho_F) + \Phi_{PX}\varphi_{PX}\Delta\rho_\varphi \quad (1)$$

with α, ρ, ρ_m, T, T_m, F_{EC}, $\Delta\rho_F$, $\Delta\rho_\varphi$, φ_{EC}, and φ_{PX} the thermal expansivity, density, reference mantle density (3300 kg/m³), temperature, reference temperature, depletion of EC, density anomaly related to 100% depletion (−165 kg/m³ (Schutt and Lesher, 2006)), and density anomaly of magma (−500 kg/m³), porosity in EC and in PX, respectively. Herein, we neglect the effects of depletion of DC F_{DC} on density. This assumption is valid as long as the residual harzburgitic layer from DC-melting at the MOR (HL) remains effectively undisturbed by SSC and the DC solidus is not crossed in the model domain, conditions that are validated a posteriori. Furthermore, we take the density anomaly related to pyroxenite to be zero, as the density of pyroxene is close to ρ_m.

We apply a Newtonian rheology dependent on temperature, depth, and composition:

$$\eta = \eta_m \Pi_{DC}^{\Phi_{DC}/(\Phi_{DC}+\Phi_{EC})} \Pi_{EC}^{\Phi_{EC}/(\Phi_{EC}+\Phi_{DC})} \exp\left(\frac{E^*+\rho_m g z V^*}{RT} - \frac{E^*}{RT_m}\right) \quad (2)$$

with

$$\Pi_{DC} = \frac{\xi(c_{0,DC}-c_{dry})}{(c_{DC}-c_{dry})\xi + c_{0,DC}-c_{DC}}, \quad (3)$$

and

$$\Pi_{EC} = \frac{\xi(c_{0,EC}-c_{dry})\exp(\zeta\varphi_{EC})}{(c_{EC}-c_{dry})\xi + c_{0,EC}-c_{EC}}, \quad (4)$$

where ζ, η, η_m, g, z, R, E^*, V^*, c_{DC} and c_{EC} are, the melt lubrication exponent, viscosity, reference viscosity, gravity acceleration, depth, the ideal gas constant, activation energy, activation volume, water content in the solid of DC and of EC, respectively. We take $\zeta=-40$ (Kohlstedt and Zimmerman, 1996), $V^*=5$ cm³/mol (Karato and Wu, 1993), and $E^*=120$ kJ/mol (in order to mimic the effects of dislocation creep in the asthenosphere with Newtonian rheology (Christensen, 1984; van Hunen et al., 2005)). Eq. (2) is a standard formulation for Newtonian rheology with geometrically averaged terms for compositional rheology of DC and EC (i.e., Π_{DC} and Π_{EC}; Fig. 2c shows a profile of the bulk compositional rheology), which are both based on the following considerations: (1) viscosity is inversely proportional to water content (e.g., Karato and Wu, 1993). (2) The associated viscosity jump between undepleted (i.e., solid water content c is that in the starting source c_O) and dry (for $c\leq c_{dry}=0.0006$ wt.%) peridotite is taken to be $\xi=100$ (Hirth and Kohlstedt, 1996). (3) Melt lubrication in EC is treated according to Kohlstedt and Zimmerman (1996). Melt lubrication and dehydration stiffening in pyroxenite are ignored, since the rheology of a multi-lithological assemblage is dominated by that of the matrix (Φ_{PX} is 4% at most). Since the HL is assumed to remain unperturbed by SSC (i.e., c_{DC} is laterally uniform), rheology ultimately depends on T, z, c_{EC}, and φ_{EC} only.

The initial compositional structure of the mantle further controls some of the main model predictions. We assume that the oceanic upper mantle has already been processed by partial melting at a MOR; therefore we perform separate 2D calculations of melting and lithosphere accretion at a MOR. By applying the same T_m, $\Phi_{PX,i}$, Φ_{EC}, and Φ_{DC} at the MOR as within the model domain, we assume that the MOR (i.e., the East Pacific Rise) is influenced by the broad SP Superswell (e.g., Toomey et al., 2002). The vertical profiles of the depletions of DC, EC and PX (i.e., F_{DC}, F_{EC} and F_{PX}) after MOR melting (Fig. 2) are then used as the initial as well as the inflow boundary conditions in the 3D-models.

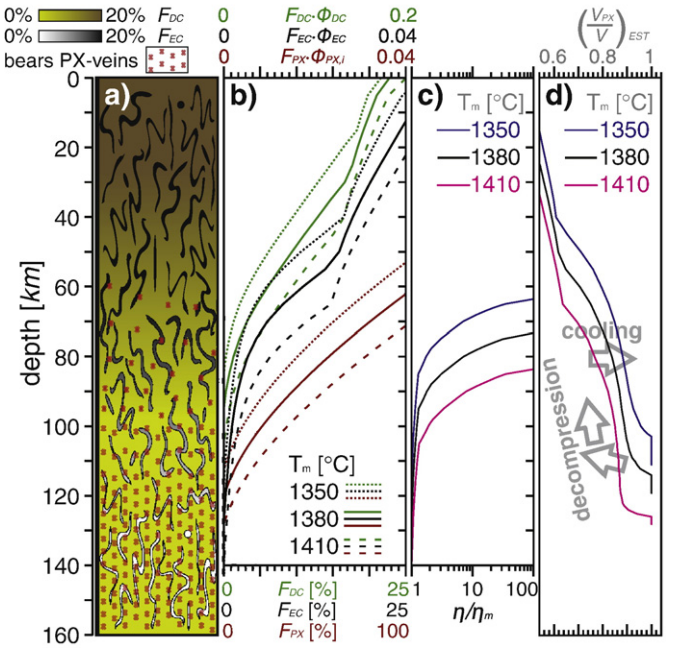

Fig. 2. (a) Schematic of the initial compositional stratification for $T_m=1380$ °C as inherited from MOR melting. (b) Initial depletion profiles for various T_m. PX ($\Phi_{PX,i}=4\%$) and EC ($\Phi_{EC}=16\%$) begin melting deepest, followed by DC. The extents of melting for PX and EC above the DC solidus are overestimated, as the effects of latent heat consumption in DC at the MOR on PX- and EC-melting are ignored. However, this does not affect our results, as these shallow levels do not participate in SSC (shallowest depths of SSC-melting are 83, 92, and 100 km for $T_m=1350$, 1380 and 1410 °C, respectively). (c) Compositional viscosity profile as derived from the initial depletion profiles and Eqs. (3) and (4). (d) Profiles of the estimated share of PX-derived melts in the total melt volume flux, $(V_{PX}/V)_{EST}$, for different T_m. Arrows show schematic evolution of compositions as SSC strengthens ("decompression") and wanes with "cooling" (see text and Eq. (5)).

3. Results of numerical models

We study SSC and related melting of a veined mantle source by exploring numerical models within a parameter space. We vary reference mantle temperature T_m from 1350 to 1440 °C, and effective viscosity η_{eff} from $0.9{\cdot}10^{19}$ to $1.8{\cdot}10^{19}$ Pa s. Hereby, η_{eff} as a more applicable parameter replaces η_m, and is tuned such that η_{eff} corresponds to the minimum viscosity in the mantle column at the onset of SSC ($\eta_{eff} \equiv 0.0353\eta_m$). The explored range for η_{eff} is chosen such that the predicted seafloor ages during SSC volcanism correspond to the observed ages. Calculations run until a statistical steady-state is reached. As SSC is a time-dependent mechanism with strong resulting fluctuations (e.g. ~20% for melting rate), we average results over ~50 Myrs.

The age of the seafloor under which SSC first occurs (i.e., onset age), is a function of both the vertical density and vertical viscosity profiles for a given η_{eff} (Conrad and Molnar, 1999; Zaranek and Parmentier, 2004; cf. Fig. 2c). Stiffening due to dehydration in DC inhibits SSC within the harzburgitic layer (cf. Lee et al., 2005; Afonso et al., 2008). Furthermore, stable density stratification in F_{EC} further delays SSC (cf. Eq. (1)). As thicker lids of depletion of DC and of EC produce more stable viscosity and density stratification, onset ages positively correlate with the thicknesses of these lids (cf. Ballmer et al., 2009) — and hence onset ages also with T_m (cf. Fig. 2b).

Overturn of the initial compositional stratification by SSC allows subsequent melting (Fig. 2a; Appendix). Soon after its onset, SSC removes a thin layer directly beneath the harzburgitic layer, and subsequently replaces this cooler, partially depleted (in EC and PX but not in DC) material with hotter and fresh mantle from below (Fig. 3). This continuous replacement causes decompression melting above the upwelling limbs of SSC. Since SSC takes the pattern of rolls aligned by plate motion, melting zones are elongated with the long axis parallel to plate motion ('hot line'). The total magma volume flux per km of plate width perpendicular to plate motion V is the sum of that from EC and from PX ($V = V_{EC} + V_{PX}$).

SSC volcanism can be subdivided into three characteristic stages. During the initial stage, V remains small as only supplied by relatively deep melting. However, V increases strongly towards older seafloor (Fig. 4a, b), because of intrinsic melt buoyancy driving convection (cf. Tackley and Stevenson (1993), Eq. (1)). In the second and main stage, V is large and reaches a maximum at ~8 Myrs after the onset of SSC. During the final stage, the melting zone is constricted as the circulating mantle has cooled by the sublithospheric material it has incorporated (greenish colors in Fig. 3). This process ultimately terminates volcanism. V as integrated over all stages is sufficient to produce seamounts with total crustal thicknesses of ~5 km (numbers in Fig. 4a) for the parameter space explored.

The lithologic make-up of the extracted melts differs between the three volcanic stages owing to the changing depths and extents of decompression melting (Fig. 4c). The share of PX-derived melts in the total magma volume flux (V_{PX}/V) is typically 90%–100% during the initial stage, it decreases to 60%–80% during the main stage (i.e., when V is greatest), and then rises back to 90%–100% during final stage. The volumetrically averaged V_{PX}/V is close to that of the main stage (i.e., 60%–80%), because most of the melt flux occurs during this stage. That $V_{PX}/V > 50\%$ (i.e., $V_{PX} > V_{EC}$) throughout each model is due to greater maximal extents of melting in PX than in EC (~25% vs. ~2.5%).

A simplified analysis elucidates the underlying mechanisms for the typical evolution of V_{PX}/V over seafloor ages. For an adiabatically decompressing parcel of mantle, the 'normalized extents of melting' of each lithology (i.e., $F_{EC}{\cdot}\Phi_{EC}$ and $F_{PX}{\cdot}\Phi_{PX,i}$) as a function of depth are given in Fig. 2b. From these profiles, we estimate the PX melt contribution, $(V_{PX}/V)_{EST}$, as a function of the minimal depth reached by SSC-upwellings after subtracting the absolute magma fraction retained in the mantle (i.e., $\varphi_C{\cdot}\Phi_{EC}$ and $\varphi_C{\cdot}\Phi_{PX,i}$):

$$(V_{PX}/V)_{EST} = \frac{\Phi_{PX,i}(F_{PX} - \varphi_C)}{\Phi_{PX,i}(F_{PX} - \varphi_C) + \Phi_{EC}(F_{EC} - \varphi_C)} \quad (5)$$

Fig. 2d displays $(V_{PX}/V)_{EST}$ versus depth. During the initial stage of volcanism, when melts are formed deepest, $(V_{PX}/V)_{EST}$ is high (starting from 100%), because F_{PX} exceeds φ_C deeper than F_{EC} does. During the main stage, SSC-melting proceeds to shallower levels and enhanced EC-melting lowers $(V_{PX}/V)_{EST}$ (cf. arrows 'decompression' in Fig. 2d). During final stage, asthenospheric cooling reduces EC-melting more than PX-melting and hence increases $(V_{PX}/V)_{EST}$ (cf. trend between different curves in Fig. 2d).

Fig. 4c further shows that the minimum or mean V_{PX}/V systematically decreases with T_m — and hence V_{PX}/V also with the average seafloor age during volcanism. This systematic is consistent

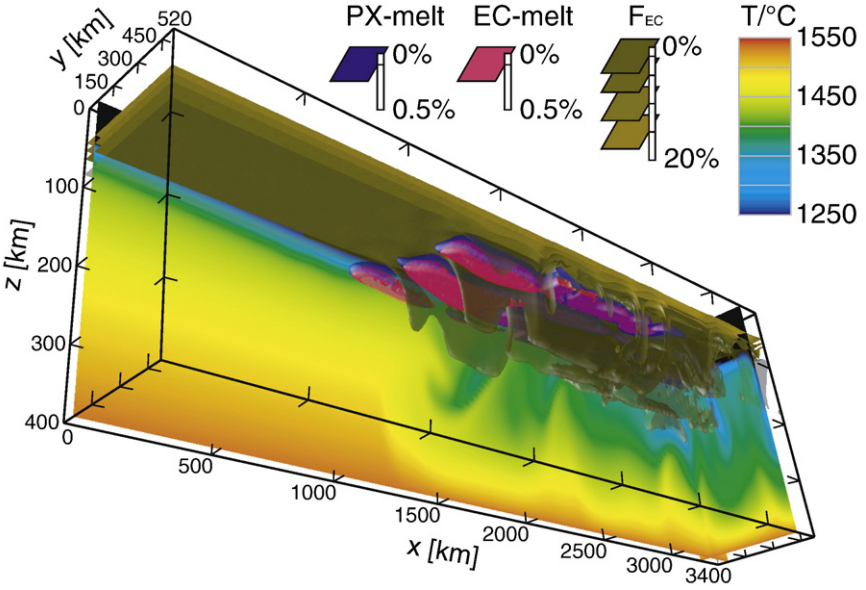

Fig. 3. Isosurfaces of φ_{EC} (at 0.1%), of φ_{PX} (at 0.1%), and of F_{EC} (at 1.5%, 5%, 10%, and 15%), as well as cross-sections of the temperature field for an example calculation (with $T_m = 1380$ °C and $\eta_{eff} = 1.2{\cdot}10^{19}$ Pa s). Downwelling sheets remove the bottom of the partially depleted (in PX and EC) layer from MOR melting and upwellings replace it with undepleted mantle from below. Melting stretches along the upwellings parallel to plate motion.

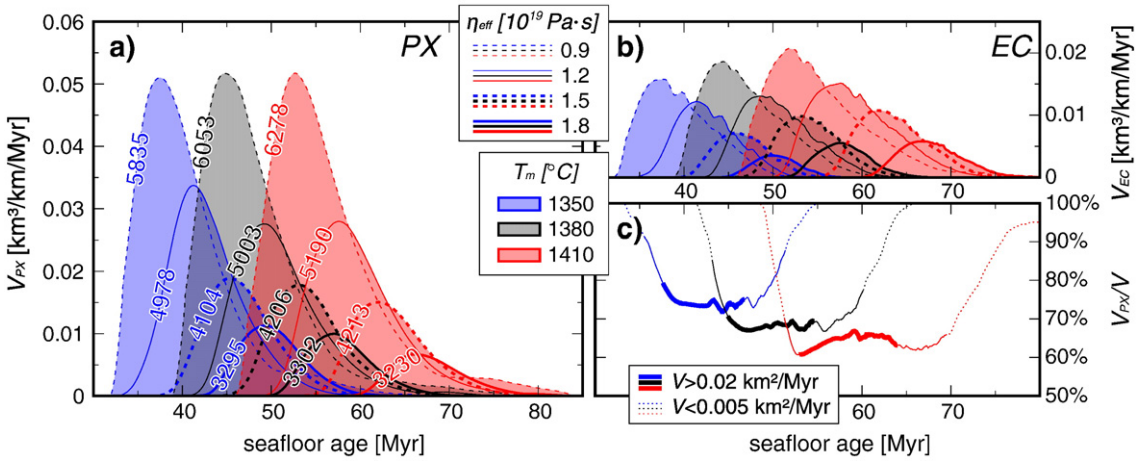

Fig. 4. Melt volume flux of (a) V_{PX}, and (b) V_{EC} of volcanism versus seafloor ages. Predictions for different reference viscosities and temperatures (η_{eff} and T_m) are shown. Volume fluxes are most sensitive to η_{eff}, whereas seafloor ages during volcanism are most sensitive to T_m. The area beneath each curve in a and b is proportional to the cumulative melt column height from PX- and EC-melting, respectively. Numbers in a represent the sum of these heights translated into total crustal thicknesses [m] of virtual volcanoes with slopes of 10° and separated by 100 km. (c) The share of PX-derived melts out of the total flux (i.e., V_{PX}/V with $V = V_{PX} + V_{EC}$) for models with $\eta_{eff} = 1.2 \cdot 10^{19}$ Pa s. Different line types (bold, thin, and dotted) flag periods with different total volcanic fluxes.

with the simplified analysis above: $(V_{PX}/V)_{EST}$ at the minimum depth reached by SSC-upwellings decreases with increasing T_m, a result that is ultimately caused by the solidus depth of EC being more sensitive to T_m than that of PX.

4. Comparison of model predictions with observations

4.1. Geochronology

A key prediction of our models is that simultaneous volcanism occurs over a wide distance in the direction of plate motion. The typical length of the zone of active volcanism ('hot line') extends ~1500 km (cf. Fig. 4). The age–distance relationships from such a 'hot line' are therefore likely to be complex (Ballmer et al., 2009). Instead of following a line in age–distance, the volcanoes should plot in a broad swath, ~1500 km wide in distance (shaded fields in Fig. 5). Thus, SSC reconciles both synchronous volcanism over large distances and persistent activity of 20–25 Myrs at a single volcano.

These predictions are in accord with observations at the Wakes, Marshalls, Gilberts, and Cook-Australs (Davis et al., 1989; Chauvel et al., 1997; Koppers et al., 1998, 2003; Bonneville et al., 2006). For each individual chain of these volcano groups (distinct symbols in Fig. 5), and for all chains of each group projected on top of each other, most sample ages plot within fields of width ~1500 km in age–distance space. For the Cook-Australs, the distribution of ages vs. distance can be interpreted as representing two episodes of SSC

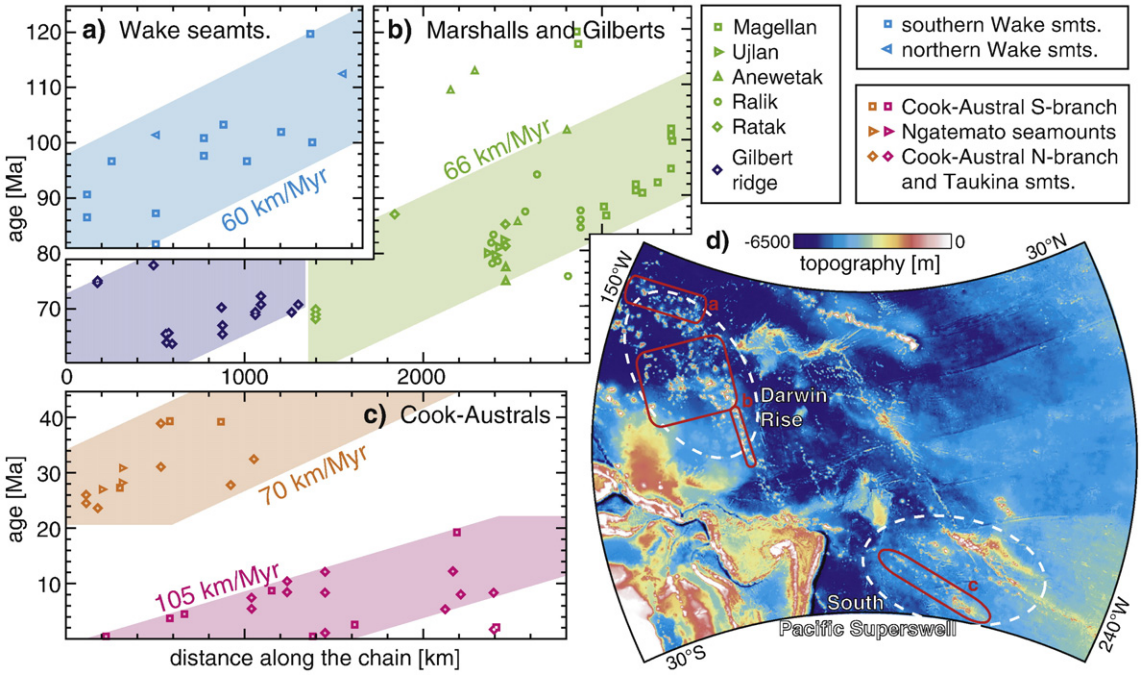

Fig. 5. Ages vs. distance for the (a) Wake seamounts, the (b) Marshalls/Gilberts, and the (c) Cook-Austral Islands compared to the predictions of the SSC hypothesis (colored fields of width ~1500 km). The Cook-Austral data can be explained with two distinct episodes of SSC-melting (pink and orange fields). Locations of the volcano chains on the Pacific Plate are given in d. Ages are taken from Koppers et al. (2003; 2007), Duncan and McDougall (1976), Turner and Jarrard (1982), Chauvel et al. (1997), McNutt et al. (1997), and Bonneville et al. (2006).

volcanism: an earlier episode (40–20 Ma) as formed on young seafloor (10–35 Myrs old) and a recent episode (≤20 Ma) on older seafloor (50–90 Myrs old). A more detailed analysis is given in Ballmer et al. (2009).

Beyond age constraints, additional observations support the SSC hypothesis. Seafloor ages during volcanism at the WPSP and the recent episode of the Cook-Australs (both 50–90 Myrs) are generally in accord with our model predictions for 1380 °C ≤ T_m ≤ 1440 °C. Moreover, typical volcano heights of ~5 km are consistent with our model predictions for low η_{eff}. Finally, the spacing between the individual parallel chains of each volcano group of about 200–300 km agrees with the typical wavelength of SSC predicted (which is a function of η_{eff}, but does not significantly vary throughout the parameter space).

4.2. Geochemistry

A robust prediction of our models is that the lithologic origin of lavas systematically varies with the age of the seafloor, on which they erupt (Fig. 4c). To relate these predictions with geochemical observations, we associate each lithology with a radiogenic isotope characteristic. Radiogenic isotope ratios are a good measure of the source material melting because isotopes are not fractionated during partial melting. The global arrays of OIBs in the multidimensional radiogenic isotope space are bound by 4 end-members: DMM, EM1, EM2 and HIMU (Zindler and Hart, 1986; Hart et al., 1992). While the specific origin of these geochemical end-members remains debated, we assume that PX and EC have an isotopic composition similar to HIMU (Hirschmann et al., 2003; Kogiso and Hirschmann, 2006) and EM1 (Jackson and Dasgupta (2008), and references therein), respectively. Accordingly, our numerical models predict systematic and distinct variations of isotope ratios in basalts (between end-members HIMU and EM1) with seafloor age along each chain.

Fig. 6a shows that isotope ratios collected along the Wakes, Marshalls, Gilberts and the recent episode of the Cook-Australs indeed stretch out between the mantle end-members HIMU and EMI in $^{87}Sr/^{86}Sr$ and $^{206}Pb/^{204}Pb$ space (Staudigel et al., 1991; Koppers et al., 2003). After scaling the axes with the field spanned by the end-member compositions (grey box in Fig.6a), we project each data-point onto an axis connecting HIMU and EMI (not shown in Fig. 6a) in order to obtain a measure for the strength of the HIMU geochemical signature: χ, for which $\chi = 100\%$ for HIMU and $\chi = 0\%$ for EMI. Considering at least two isotope systems is essential in order to achieve an adequate degree of accuracy of this approach. $^{87}Sr/^{86}Sr$ and $^{206}Pb/^{204}Pb$ are our favored choice because they provide the largest set of samples for which isotopic ratios are measured, and because these two systems show some of the largest variations between HIMU and EMI (Allègre et al., 1987; Hart et al., 1992).

The Gilberts, Marshalls, and Cook-Australs display systematic geochemical trends over the age of the seafloor on which volcanoes were formed (Fig. 6b). Wide portions of the data show the HIMU signature χ of basalts increasing with age (e.g., Wake at seafloor ages 50–70 Myrs, Cook-Austral 50–80 Myrs, Gilberts 50–80 Myrs, and Marshalls, 70–100 Myrs; dashed lines Fig. 6b). These positive trends in χ are consistent with our model predictions, which show slight increases in V_{PX}/V with seafloor age during main stages, and steep increases during final stages of SSC volcanism (solid curves in Fig. 6b). Thereby, it is realistic that the initial stage is underrepresented in the geochemical dataset, as it is likely to be buried beneath later stage volcanism (maybe except for the Wakes).

There are also trends in differences between chains. In comparing χ between chains at a fixed seafloor age, we see that χ of the Gilberts is similar to χ of Cook-Australs (formed on seafloor ages of 40–80 Myrs), but systematically lower than χ of the Wakes and higher than χ of the Marshall Islands (cf. dashed curves in Fig. 6b). Thus, χ of the individual chains appear to shift toward lower values for older seafloor at the time of volcanism. These observations are broadly consistent with the predictions of our numerical model for how V_{PX}/V differs with increasing T_m (different solid curves Fig. 6b). Along these lines, the data reveals a dominant dynamical process of melting the same veined mantle source — rather than indicating random sampling of strong compositional heterogeneity (cf. Janney and Castillo, 1999; Konter et al., 2008).

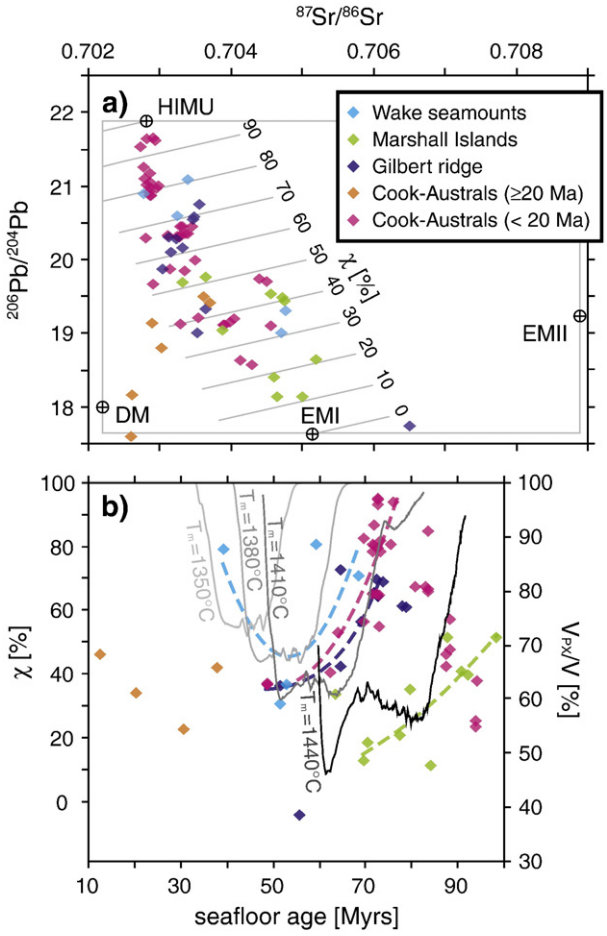

Fig. 6. (a) Radiogenic isotope correlation for ocean island basalts ($^{87}Sr/^{86}Sr$ vs. $^{204}Pb/^{204}Pb$) organized by volcano chain, and in the case of the Cook-Australs also by age. Isotope data for the Cook-Australs are from Chauvel et al. (1997), Schiano et al. (2001) and Bonneville et al. (2006); end-member compositions and all other data are from Konter et al. (2008) and references therein. The $^{87}Sr/^{86}Sr$–$^{204}Pb/^{204}Pb$ composition is represented by χ as graphically derived (grey lines; for details see text). (b) χ vs. age of the seafloor during volcanism (as obtained from subtracting seafloor ages of Muller et al. (2008) from volcano ages). Dashed curves are quadratic regressions (ignoring some outliers for the Gilberts). For comparison, numerical model predictions in terms of V_{PX}/V are given for various T_m and for $\eta_{eff} = 1.2 \cdot 10^{19}$ Pa s (solid curves; only at $V > 10^{-4}$ km^3/km/Myr).

Taken together, the data from the Cook-Austral Islands cannot be explained by a single set of physical properties of the mantle. Volcanism on seafloor younger than 40 Myrs (earlier episode; orange colors in Figs. 5, 6) is not predicted by our set of numerical calculations rather requiring lower η_{eff} than modeled. Such a model probably would involve partial melting of the DC-matrix (Ballmer et al., 2009), which his not simulated here (cf. Section 2). Indeed, radiogenic isotope ratios of these basalts plot between C/FOZO (not shown in Fig. 6a) and DMM (orange branch in Fig. 6a), an observation that is consistent with melting of DC (e.g., Hart et al., 1992). The Cook-Austral data spanning seafloor ages of 50–80 Myrs is predicted by our models with $T_m \approx 1410$ °C (cf. Fig. 6b). In contrast, the volcanism on seafloor ages >80 Myrs with low χ requires locally higher T_m of ~1440 °C (black curve in Fig. 6b), or locally higher volatile contents in

EC (not modeled). Such a complex scenario is not unrealistic, as these three populations of volcanoes have been erupted at different times, or locations relative to the Superplume.

5. Discussion

Volcanism on the South Pacific (SP) Superswell, and its precursor, the Darwin Rise has been previously attributed to secondary plumelets, and its geochemical variability to intermediate-scale (~1000 km) domains of source heterogeneity (Staudigel et al., 1991; Davaille, 1999; Janney and Castillo, 1999; Koppers et al., 2003; Konter et al., 2008). However, the invoked persistency of these domains (>100 Myrs) has not yet been shown to be consistent with the typical timescale of plumelets (~30 Myrs). Here, we have shown a positive test for the SSC hypothesis (Fig. 6b). SSC reconciles the previous enigma of widely scattered age–distance relations, it explains a huge range of the observed $^{87}Sr/^{86}Sr$ and $^{206}Pb/^{204}Pb$ compositions, and it does so for the appropriate range of seafloor ages at the time of volcanism. Overall, SSC requires minimal intermediate-scale zoning in composition and some variations in mantle temperature to explain the data considered.

In the extreme situation of a perfectly uniform average mantle composition (with vein-size heterogeneities), SSC would require temporal changes in mantle temperature T_m to satisfy geochemical constraints. Our models demonstrated that increases of T_m systematically shift geochemical trends associated with SSC volcanism towards EMI, and towards higher seafloor ages. Thus, the distinct evolutions of χ over seafloor ages (Fig. 6b) suggest that magmas making up the Gilberts and part of the Cook-Australs were generated in a cooler environment than those making up the Marshalls, and in a hotter environment than those making up the Wakes. This interpretation implies temporal changes of T_m in the specific mantle domain, from which all the discussed volcano chains were fed (cf. Bonneville et al., 2006): from relatively low T_m (~1380 °C) at 110–90 Ma, when most of the Wakes have been formed, to high T_m (~1440 °C) at 100–75 Ma (Marshalls), back to intermediate T_m (~1400 °C) at 75–60 Ma (Gilberts) and at 20–0 Ma (recent episode of the Cook-Australs). We speculate that such changes arise from the complex interaction of the Superplume with the transition zone with subsequent pulses of Superplume activity in the upper mantle (cf. Adam and Bonneville, 2005).

The most important requirement for volcanism to occur from SSC is a sufficiently early onset age of 30–55 Myrs. However, SSC is typically thought to develop beneath seafloor of ages ~70 Myrs (e.g., Doin and Fleitout, 2000). This discrepancy complicates volcanism from SSC in most ocean basins. In the SP, however, the abundant thermal anomaly likely reduces the onset of SSC by both reducing the viscosity in the upper mantle, and providing lateral thermal density heterogeneity (Richter and Parsons, 1975; Huang et al., 2003; Dumoulin et al., 2008). Accordingly, SSC tends to be triggered at the edges of the SP Superswell (Griffiths and Campbell, 1991). Such a situation partly explains the unusually high frequency of intraplate volcanism in the SP.

Volcanism from SSC further presupposes a fertile mantle source as abundant in the SP (Staudigel et al., 1991). In our models, we used a fixed source composition that was chosen somewhat arbitrarily (i.e.: $\Phi_{DC}=80\%$; $\Phi_{EC}=16\%$; $\Phi_{PX,i}=4\%$). Source compositions with a similar $\Phi_{EC}/\Phi_{PX,i}$ but a higher Φ_{DC} than modeled likely yield smaller amounts of volcanism than predicted. The ratio of Φ_{EC}/Φ_{PX} directly controls the mean V_{PX}/V, for which our models predict to range between 60% and 80%. Results from experimental petrology indicate that alkalic OIBs like those samples from the WPSP and the Cook-Australs can indeed be derived from PX-melting mainly (Hirschmann et al., 2003; Kogiso and Hirschmann, 2006). Our model predictions of mean V_{PX}/V can further be tested by Mn/Fe-ratios of picked olivines from Woodebajato seamount in the Marshall Islands. Application of the scheme of Sobolev et al. (2007) on least ferrous Woodebajato olivines (i.e., Fo84–Fo85) (Dieu, 1995) yields a mean $V_{PX}/V\approx70\%$, which falls within the range of our model predictions.

The consideration of only three lithologies (DC, EC and PX) and one volatile phase (i.e., H_2O) is another limitation. Other lithologies such as hornblendite veins and volatiles such as CO_2 likely play a crucial role for the generation of alkalic OIBs (Niu and O'Hara, 2003; Dasgupta et al., 2007; Pilet et al., 2008). These simplifications indeed limit the predictive power of our models in terms of minor and major element geochemistry of magmas, but they do not invalidate dynamic melting processes, because CO_2 and hornblendite veins play a similar role in shifting the solidus as H_2O and PX do, respectively (Katz et al., 2003 vs. Dasgupta et al., 2007; S. Pilet, pers. comm., 2009).

Our results highlight that accounting for the dynamical processes of partial melting is of utmost importance to understand geochemical trends along ocean island chains. Considering a veined mantle source, Ito and Mahoney (2005b) revealed that these processes produce large geochemical differences between distinct chains with relatively small variations in source composition. In support of the veined mantle hypothesis, we and Bianco et al. (2008) showed in 3D-numerical models of SSC and of plumes, respectively, that melting processes may further account for geochemical variations within individual volcano groups.

6. Conclusions

Numerical models show that SSC that initiates beneath sufficiently young seafloor gives rise to decompression melting of fertile lithological components (i.e., enriched peridotite and pyroxenite) within its upwelling limbs. Resulting volcanism potentially emerges synchronously along a zone of length ~1500 km parallel to plate motion ('hot line') on intermediate seafloor ages (i.e., 35–90 Myrs). Therefore, age–distance patterns along the associated volcanic chains are expected to be complex. The share of pyroxenite-derived lavas in the total melt volume flux (V_{PX}/V) is predicted to be of the order of 70% and to vary along the 'hot line' with lowest V_{PX}/V above its center and highest $V_{PX}/V>90\%$ towards its ends. Variation of V_{PX}/V along an individual 'hot line' implies a systematic geochemical trend vs. seafloor age during volcanism. Higher mantle temperatures are predicted to shift this geochemical trend towards higher seafloor ages and lower V_{PX}/V.

These predictions reconcile both complex age–distance relationships, and many of the radiogenic isotope trends as observed along the Wakes, Marshalls, Gilberts, and Cook-Australs. The specific differences in the observed isotopic trends between the distinct chains can further be explained by temporal variation of mantle temperature within the source region. Thus, SSC explains the timing and composition of volcanism in the West and South Pacific without presuming the repeated sampling of the same distinct geochemical source domains over ~100 Ma by short-lived plumelets.

Acknowledgements

M. Ballmer was sponsored by SNF projects 20021-107995/1 and 20020-119922/1, and G. Ito was supported by NSF grants EAR-0040365 and EAR-0510482. We thank S. King and an anonymous reviewer for their comments that greatly helped to improve this manuscript.

Appendix A. Supplementary data

Supplementary data associated with this article can be found, in the online version, at doi:10.1016/j.epsl.2009.12.025.

References

Adam, C., Bonneville, A., 2005. Extent of the South Pacific Superswell. Journal of Geophysical Research—Solid Earth 110.

Afonso, C.A., Zlotnik, S., Fernandez, M., 2008. Effects of compositional and rheological stratifications on small-scale convection under the oceans: implications for the thickness of oceanic lithosphere and seafloor flattening. Geophysical Research Letters 35.

Allègre, C.J., Hamelin, B., Dupré, B., 1984. Statistical analysis of isotopic ratios in MORB: the mantle blob cluster model and the convective regime of the mantle. Earth and Planetary Science Letters 71, 71–84.

Allègre, C.J., Hamelin, B., Provost, A., Dupre, B., 1987. Topology in isotopic multispace and origin of mantle chemical heterogeneities. Earth and Planetary Science Letters 81, 319–337.

Anderson, D.L., 2000. The thermal state of the upper mantle; no role for mantle plumes. Geophysical Research Letters 27, 3623–3626.

Ballmer, M.D., van Hunen, J., Ito, G., Bianco, T.A., Tackley, P.J., 2009. Intraplate volcanism with complex age–distance patterns — a case for small-scale sublithospheric convection. Geochemistry, Geophysics, Geosystems 10.

Ballmer, M.D., van Hunen, J., Ito, G., Tackley, P.J., Bianco, T.A., 2007. Non-hotspot volcano chains originating from small-scale sublithospheric convection. Geophysical Research Letters 34.

Bianco, T.A., Ito, G., van Hunen, J., Ballmer, M.D., Mahoney, J.J., 2008. Geochemical variation at the Hawaiian hot spot caused by upper mantle dynamics and melting of a heterogeneous plume. Geochemistry Geophysics Geosystems 9.

Bonatti, E., Harrison, C.G.A., 1976. Hot lines in the Earth's mantle. Nature 263, 402–404.

Bonneville, A., Dosso, L., Hildenbrand, A., 2006. Temporal evolution and geochemical variability of the South Pacific superplume activity. Earth and Planetary Science Letters 244, 251–269.

Buck, W.R., Parmentier, E.M., 1986. Convection beneath young oceanic lithosphere: implications for thermal structure and gravity. Journal of Geophysical Research 91, 1961–1974.

Cadek, O., Fleitout, L., 2003. Effect of lateral viscosity variations in the top 300 km on the geoid and dynamic topography. Geophysical Journal International 152, 566–580.

Chauvel, C., McDonough, W., Guille, G., Maury, R., Duncan, R., 1997. Contrasting old and young volcanism in Rurutu Island, Austral chain. Chemical Geology 139, 125–143.

Christensen, U., 1984. Convection with pressure-dependent and temperature-dependent non-Newtonian rheology. Geophysical Journal of the Royal Academy of Science 77, 343–384.

Christensen, U.R., Yuen, D.A., 1985. Layered convection induced by phase transitions. Journal of Geophysical Research 90, 10,291–10,300.

Clouard, V., Bonneville, A., 2005. Ages of seamounts, islands, and plateaus on the Pacific plate. Plumes, Plates, and Paradigms, Special Paper - Geological Society of America 388, 71–90.

Clouard, V., Gerbault, M., 2008a. Break-up spots: could the Pacific open as a consequence of plate kinematics? Earth and Planetary Science Letters 265, 195–208.

Clouard, V., Gerbault, M., 2008b. Reply to “Break-up spots: Could the Pacific open as a consequence of plate kinematics?” Comment by R. Pilger. Earth and Planetary Science Letters 275, 196–199.

Conrad, C.P., Molnar, P., 1999. Convective instability of a boundary layer with temperature- and strain-rate-dependent viscosity in terms of “available buoyancy”. Geophysical Journal International 139, 51–68.

Courtillot, V., Davaille, A., Besse, J., Stock, J., 2003. Three distinct types of hotspots in the Earth's mantle. Earth and Planetary Science Letters 205, 295–308.

Dasgupta, R., Hirschmann, M.M., Smith, N.D., 2007. Partial melting experiments of peridotite CO2 at 3 GPa and genesis of alkalic ocean island basalts. Journal of Petrology 48, 2093–2124.

Davaille, A., 1999. Simultaneous generation of hotspots and superswells by convection in a heterogeneous planetary mantle. Nature 402, 756–760.

Davis, A.S., Pringle, M.S., Pickthorn, L.B.G., Clague, D.A., Schwab, W.C., 1989. Petrology and age of alkalic lava from the Ratak chain of the Marshall Islands. Journal of Geophysical Research—Solid Earth and Planets 94, 5757–5774.

Dieu, J.J., 1995. Mineral compositions in Leg 144 lavas and ultramafic xenoliths: the roles of cumulates and carbonatite metasomatism in magma petrogenesis. Proceedings of the Ocean Drilling Program 144, 513–533.

Doin, M.P., Fleitout, L., 2000. Flattening of the oceanic topography and geoid: thermal versus dynamic origin. Geophysical Journal International 143, 582–594.

Dumoulin, C., Choblet, G., Doin, M.P., 2008. Convective interactions between oceanic lithosphere and asthenosphere: influence of a transform fault. Earth and Planetary Science Letters 274, 301–309.

Duncan, R.A., McDougall, I., 1976. Linear volcanism in French Polynesia. Journal of Volcanology and Geothermal Research 1, 197–227.

Fleitout, L., Yuen, D.A., 1984. Secondary convection and the growth of the oceanic lithosphere. Physics of the Earth and Planetary Interiors 36, 181–212.

Foulger, G.R., 2007. The “Plate” model for the origin of melting anomalies. In: Foulger, G.R., Jurdy, D.M. (Eds.), Plates, Plumes, and Planetary Processes: Geological Society of America, pp. 1–28.

Griffiths, R.W., Campbell, I.H., 1991. Interaction of mantle plume heads with the Earth's surface and onset of small-scale convection. Journal of Geophysical Research—Solid Earth 96, 8295–8310.

Hanan, B.B., Graham, D.W., 1996. Lead and helium isotope evidence from oceanic basalts for a common deep source of mantle plumes. Science 272, 991–995.

Hart, S.R., Hauri, E.H., Oschmann, J.A., Whitehead, J.A., 1992. Mantle plumes and entrainment: isotopic evidence. Science 256, 517–520.

Hirschmann, M.M., Kogiso, T., Baker, M.B., Stolper, E.M., 2003. Alkalic magmas generated by partial melting of garnet pyroxenite. Geology 31, 481–484.

Hirth, G., Kohlstedt, D.L., 1996. Water in the oceanic upper-mantle — implications for rheology, melt extraction and the evolution of the lithosphere. Earth and Planetary Science Letters 144, 93–108.

Huang, J.S., Zhong, S.J., van Hunen, J., 2003. Controls on sublithospheric small-scale convection. Journal of Geophysical Research 108, 2405.

Ito, G., Mahoney, J.J., 2005a. Flow and melting of a heterogeneous mantle: 1.Method and importance to the geochemistry of ocean island and mid-ocean ridge basalts. Earth and Planetary Science Letters 230, 29–46.

Ito, G., Mahoney, J.J., 2005b. Flow and melting of a heterogeneous mantle: 2. Implications for a chemically nonlayered mantle. Earth Planet. Sci. Lett. 230, 47–63.

Jackson, M.G., Dasgupta, R., 2008. Compositions of HIMU, EM1, and EM2 from global trends between radiogenic isotopes and major elements in ocean island basalts. Earth and Planetary Science Letters 276, 175–186.

Janney, P.E., Castillo, P.R., 1999. Isotope geochemistry of the Darwin Rise seamounts and the nature of long-term mantle dynamics beneath the south central Pacific. Journal of Geophysical Research—Solid Earth 104, 10,571–10,589.

Karato, S., Wu, P., 1993. Rheology of the upper mantle — a synthesis. Science 260, 771–778.

Katz, R.F., Spiegelman, M., Langmuir, C.H., 2003. A new parameterization of hydrous mantle melting. Geochemistry, Geophysics, Geosystems 4, 9. doi:10.1029/2002GC000433.

Keller, T., Tackley, P.J., 2009. Towards self-consistent modeling of the martian dichotomy: the influence of one-ridge convection on crustal thickness distribution. Icarus 202, 429–443.

King, S.D., 2007. Hotspots and edge-driven convection. Geology 35, 223–226.

King, S.D., Ritsema, J., 2000. African hot spot volcanism: small-scale convection in the upper mantle beneath cratons. Science 290, 1137–1140.

Kogiso, T., Hirschmann, M.M., 2006. Partial melting experiments of bimineralic eclogite and the role of recycled mafic oceanic crust in the genesis of ocean island basalts. Earth and Planetary Science Letters 249, 188–199.

Kohlstedt, D.L., Zimmerman, M.E., 1996. Rheology of partially molten mantle rocks. Annual Review of Earth and Planetary Sciences 24, 41–62.

Konter, J.G., Hanan, B.B., Blichert-Toft, J., Koppers, A.A.P., Plank, T., Staudigel, H., 2008. One hundred million years of mantle geochemical history suggest the retiring of mantle plumes is premature. Earth and Planetary Science Letters 275, 285–295.

Koppers, A.A.P., Staudigel, H., Morgan, J.P., Duncan, R.A., 2007. Nonlinear Ar-40/Ar-39 age systematics along the Gilbert Ridge and Tokelau Seamount Trail and the timing of the Hawaii-Emperor Bend. Geochemistry Geophysics Geosystems 8.

Koppers, A.A.P., Staudigel, H., Pringle, M.S., Wijbrans, J.R., 2003. Short-lived and discontinuous intraplate volcanism in the South Pacific: hot spots or extensional volcanism? Geochemistry, Geophysics, Geosystems 4, 1089. doi:10.1029/2003GC000533.

Koppers, A.A.P., Staudigel, H., Wijbrans, J.R., Pringle, M.S., 1998. The Magellan seamount trail: implications for Cretaceous hotspot volcanism and absolute Pacific plate motion. Earth and Planetary Science Letters 163, 53–68.

Larson, R.L., 1991. Latest pulse of Earth — evidence for a Midcretaceous Superplume. Geology 19, 547–550.

Lee, C.T.A., Lenardic, A., Cooper, C.M., Niu, F.L., Levander, A., 2005. The role of chemical boundary layers in regulating the thickness of continental and oceanic thermal boundary layers. Earth and Planetary Science Letters 230, 379–395.

McKenzie, D., 1985. Th-230–U-238 disequilibrium and the melting processes beneath ridge axes. Earth and Planetary Science Letters 72, 149–157.

McNutt, M.K., Caress, D.W., Reynolds, J., Jordahl, K.A., Duncan, R.A., 1997. Failure of plume theory to explain midplate volcanism in the southern Austral islands. Nature 389, 479–482.

McNutt, M.K., Fisher, K., 1987. The South Pacific Superswell. In: Keating, B., Fryer, P., Batiza, R., Boehlert, G.W. (Eds.), Seamounts, Islands, and Atolls: Geophysical Monograph AGU.

Moresi, L., Gurnis, M., 1996. Constraints on the lateral strength of slabs from 3-dimensional dynamic flow models. Earth and Planetary Science Letters 138, 15–28.

Morgan, W.J., 1972. Plate motions and deep mantle convection. Geological Society of America Memoirs 132, 7–22.

Muller, R.D., Sdrolias, M., Gaina, C., Roest, W.R., 2008. Age, spreading rates, and spreading asymmetry of the world's ocean crust. Geochemistry Geophysics Geosystems 9.

Niu, Y.L., O'Hara, M.J., 2003. Origin of ocean island basalts: a new perspective from petrology, geochemistry and mineral physics considerations. Journal of Geophysical Research 108. doi:10.1029/2002JB002048.

Parsons, B., McKenzie, D., 1978. Mantle convection and thermal structure of plates. Journal of Geophysical Research 83, 4485–4496.

Pertermann, M., Hirschmann, M.M., 2003. Partial melting experiments on a MORB-like pyroxenite between 2 and 3 GPa: constraints on the presence of pyroxenite in basalt source regions from solidus location and melting rate. Journal of Geophysical Research—Solid Earth 108.

Phipps Morgan, J., 2001. Thermodynamics of pressure release melting of a veined plum pudding mantle. Geochemistry, Geophysics, Geosystems 2 2000GC000049.

Pilet, S., Baker, M.B., Stolper, E.M., 2008. Metasomatized lithosphere and the origin of alkaline lavas. Science 320, 916–919.

Richter, F.M., Parsons, B., 1975. On the interaction of two scales of convection in the mantle. Journal of Geophysical Research 80, 2529–2541.

Ritzwoller, M.H., Lavely, E.M., 1995. 3-dimensional seismic models of the Earth's mantle. Reviews of Geophysics 33, 1–66.

Schiano, P., Burton, K.W., Dupre, B., Birck, J.L., Guille, G., Allegre, C.J., 2001. Correlated Os–Pb–Nd–Sr isotopes in the Austral-Cook chain basalts: the nature of mantle components in plume sources. Earth and Planetary Science Letters 186, 527–537.

Schutt, D.L., Lesher, C.E., 2006. Effects of melt depletion on the density and seismic velocity of garnet and spinel lherzolite. Journal of Geophysical Research 111, B05401. doi:10.1029/02003JB002950.

Sobolev, A.V., Hofmann, A.W., Kuzmin, D.V., Yaxley, G.M., Arndt, N.T., Chung, S.L., Danyushevsky, L.V., Elliott, T., Frey, F.A., Garcia, M.O., Gurenko, A.A., Kamenetsky, V.S., Kerr, A.C., Krivolutskaya, N.A., Matvienkov, V.V., Nikogosian, I.K., Rocholl, A., Sigurdsson, I.A., Sushchevskaya, N.M., Teklay, M., 2007. The amount of recycled crust in sources of mantle-derived melts. Science 316, 412–417.

Staudigel, H., Park, K.H., Pringle, M., Rubenstone, J.L., Smith, W.H.F., Zindler, A., 1991. The longevity of the South-Pacific isotopic and thermal anomaly. Earth and Planetary Science Letters 102, 24–44.

Stein, C.A., Stein, S., 1992. A model for the global variation in oceanic depth and heat-flow with lithospheric age. Nature 359, 123–129.

Stracke, A., Bourdon, B., McKenzie, D., 2006. Melt extraction in the Earth's mantle: constraints from U–Th–Pa–Ra studies in oceanic basalts. Earth and Planetary Science Letters 244, 97–112.

Tackley, P.J., Stevenson, D.J., 1993. A mechanism for spontaneous self-perpetuating volcanism on the terrestrial planets. In: Stone, D.B., Runcorn, S.K. (Eds.), Flow and Creep in the Solar System. Observations, Modeling and Theory. Kluwer, pp. 307–322.

Toomey, D.R., Wilcock, W.S.D., Conder, J.A., Forsyth, D.W., Blundy, J.D., Parmentier, E.M., Hammond, W.C., 2002. Asymmetric mantle dynamics in the MELT region of the East Pacific Rise. Earth and Planetary Science Letters 200, 287–295.

Turner, D.L., Jarrard, R.D., 1982. K–Ar dating of the Cook-Austral chain — a test of the hot-spot hypothesis. Journal of Volcanology and Geothermal Research 12, 187–220.

van Hunen, J., Zhong, S.J., Shapiro, N.M., Ritzwoller, M.H., 2005. New evidence for dislocation creep from 3-D geodynamic modeling of the Pacific upper mantle structure. Earth and Planetary Science Letters 238, 146–155.

Wolfe, C.J., McNutt, M.K., 1991. Compensation of Cretaceous seamounts of the Darwin Rise, Northwest Pacific-Ocean. Journal of Geophysical Research 96, 2363–2374.

Zaranek, S.E., Parmentier, E.M., 2004. Convective cooling of an initially stably stratified fluid with temperature-dependent viscosity: implications for the role of solid state convection in planetary evolution. Journal of Geophysical Research 109, B03409. doi:10.1029/02003JB002462.

Zhong, S., Zuber, M.T., Moresi, L., Gurnis, M., 2000. Role of temperature-dependent viscosity and surface plates in spherical shell models of mantle convection. Journal of Geophysical Research 105, 11,063–11,082.

Zindler, A., Hart, S., 1986. Geochemical geodynamics. Earth and Planetary Science Letters 14, 493–571.